



Article

Guide to a Deterministic Control of Laser Materials Processing with Dynamic Beam Shaping

Rudolf Weber ^{1,*}, Thomas Graf ¹, Kim Glumann ¹, Christian Hagenlocher ¹, Ami Spira ^{2,*}, Nina Armon ², Ehud Greenberg ², Rachel Assa ² and Eyal Shekel ²

¹ Institut für Strahlwerkzeuge (IFSW), University of Stuttgart, Pfaffenwaldring 43, 70569 Stuttgart, Germany; thomas.graf@ifsw.uni-stuttgart.de (T.G.); kim.glumann@ifsw.uni-stuttgart.de (K.G.); christian.hagenlocher@ifsw.uni-stuttgart.de (C.H.)

² Civan Advanced Technologies, Kanfei Nesharim 64, Jerusalem 9546455, Israel; nina.armon@civanlasers.com (N.A.); udi.greenberg@civanlasers.com (E.G.); rachel.assa@civanlasers.com (R.A.); eyal.shekel@civanlasers.com (E.S.)

* Correspondence: rudolf.weber@ifsw.uni-stuttgart.de (R.W.); ami.spira@civanlasers.us (A.S.)

Abstract

Dynamic beam shaping opens new possibilities for improving the quality and productivity of industrial laser material processing applications such as welding and cutting. However, dynamic beam shaping involves time constants and frequencies that must be selected correctly to successfully modify a given laser process. This paper proposes a standardized nomenclature for the possible types of dynamic beam shaping and the resulting dynamic process modifications, and relates these to characteristic time constants and frequencies at which the process modifications have a particularly strong influence on the process. These characteristic frequencies define three process regimes that have distinctly different effects on the process. An overview of typical time constants and frequencies in laser processes aids in understanding the occurrence of characteristic frequencies. Knowledge of the process regimes allows for a systematic selection of frequencies in dynamic beam shaping to achieve targeted dynamic process modifications, e.g., for pore reduction. Using a laser system capable of dynamic beam shaping at frequencies of up to 80 MHz, the influence of the three process zones on the porosity of the weld was demonstrated using deep welds in cast aluminum as an example.

Keywords: laser processing; laser applications; solving laser process issues; dynamic beam shaping; dynamic process modifications; dynamic beam laser (DBL)



Academic Editor: Antonio Riveiro

Received: 27 January 2026

Revised: 18 March 2026

Accepted: 22 March 2026

Published: 27 March 2026

Copyright: © 2026 by the authors.

Licensee MDPI, Basel, Switzerland.

This article is an open access article distributed under the terms and

conditions of the [Creative Commons Attribution \(CC BY\)](https://creativecommons.org/licenses/by/4.0/) license.

1. Introduction

In industrial manufacturing, the processing of a wide range of materials using high-average power continuous-wave lasers has long been established. The most important processes include hardening, in which the material remains in a solid state; cutting, in which the material is melted; and deep welding, in which partial vaporization occurs. These processes enable a broad spectrum of industrial applications as is extensively described in [1].

Significant advances have been made in recent years in both laser technology and industrial applications. On the one hand, the average power of commercially available lasers has increased significantly—from a few kilowatts in 2005 to over 100 kW by 2017 [2]. On the other hand, novel materials and improved processing techniques have paved the way for new applications. These include current progress in different industries, like the use

of high-strength alloys in crash boxes in automobiles, aluminum–copper combinations for high-current applications, such as in locomotives, and large-scale applications driven by the automotive industry’s transition to e-mobility—such as welding large aluminum cooling plates and copper hairpins for e-motors. Moreover, the trend toward mass individualization has led to a resurgence of laser-based additive manufacturing, ranging from powder- and wire-based material deposition (DED) to powder bed fusion by a laser beam (PBF-LB). All these applications pose specific challenges in terms of productivity, process stability, and the resulting quality. Key process issues include minimizing striations and dross, controlling the cutting angle when cutting thick materials, and avoiding pores, spatter, humping, and the formation of hot cracks in the solidifying material during high-speed welding.

A promising approach to address these challenges is the active forming of the intensity distribution in the focused laser beam, usually referred to as beam shaping. The beam’s intensity profile has a key influence on the energy deposition in the workpiece, and therefore, on the entire process. The irradiance distribution resulting from the beam shape and the geometry of the interaction zone on the workpiece can be used to modify process features such as widening a weld seam, influencing the heat flow or enlarging a keyhole. Illustrative examples for deep-penetration laser welding are given in [3–7]. Theoretical modeling confirmed the influence of shaped beams on the shape of the welding keyhole [8,9]. As a result, various beam shaping methods have been developed and are successfully applied to improve different aspects of the laser welding, laser cutting and additive manufacturing process, including numerical modeling [10–26]. These beam shaping systems range from static configurations to dynamic systems operating at low modulation frequencies. Comprehensive overviews of beam shaping techniques can be found in [19–21].

Dynamic beam shaping is particularly comprehensive when it enables the very rapid generation of arbitrary beam shapes. This can be achieved, for example, by actively controlling the coherent combination of the beams from many fundamental-mode lasers. Current lasers based on this principle, referred to as dynamic beam lasers (DBLs), allow for the creation of time-averaged beam shapes by quickly scanning a single, almost-fundamental mode high-intensity peak to different positions in the focal plane at frequencies of up to 80 MHz [22]. This method enables the generation of arbitrarily time-averaged beam shapes composed of a sequence of points on the workpiece surface that are scanned by an intensity peak in rapid succession, even at average powers up to 120 kW. The time-averaged beam shapes themselves can be changed with frequencies up to the MHz level, as first demonstrated in [23]. Therefore, DBLs introduce additional time constants and frequencies into dynamic beam shaping, such as the dwell time of the fundamental mode high-intensity peak at a single position, the refresh frequency of the time-averaged beam shape and the switching frequencies between the time-averaged beam shapes in a sequence of shapes.

These frequencies can be adjusted from static intensity distributions to MHz shape changes, which significantly increases the effort required for purely experimental searches for the optimal parameters for a specific process. For a systematic approach, we propose to relate the beam shaping frequencies to characteristic frequencies, which show a particularly strong response of the process. This was, for example, shown in [24], where power modulation with about 300 Hz significantly improved the welding of copper at the given process parameters. The knowledge of such characteristic frequencies is essential to allow for deterministic process modification. Based on current knowledge, it can be assumed that these characteristic frequencies are related to typical time constants and frequencies of the process, examples of which are summarized in Section 2.

In addition, the paper proposes a consistent naming of the possible types of beam shaping and process modifications and sets them in relation to characteristic time constants and frequencies. The characteristic frequencies enable the definition of three different

process regimes, which allow for targeted process modifications and support deterministic process development. An example demonstrating the occurrence of the process regimes and their influence on the welding depth and the porosity in cast aluminum is included.

2. Typical Time Constants and Frequencies in Laser Processes

The following section provides an overview of typical time constants and frequencies in laser processes. The aim is to show the range of time constants and frequencies that can be expected in laser processes. It also aims to facilitate the determination of characteristic frequencies in dynamic beam shaping, which will be described below.

2.1. Duration for Reaching a Specific Temperature on the Surface

The time required to heat the material to its melting or boiling temperature on the surface using a laser beam is of interest in every laser process. A convenient analytical approximation to estimate the temperature increase $T(0, t) - T_0$, where $T(0, t)$ is the temperature on the surface and T_0 is the initial temperature can be found in [1]. Assuming uniform heating of the surface of a semi-infinite body by the irradiance I , the temperature increase on the surface is given by

$$T(0, t) - T_0 = \frac{A \cdot I}{\lambda_{th}} \cdot \frac{\sqrt{\kappa_D \cdot t_H}}{\sqrt{\pi}}, \quad (1)$$

where A is the absorptivity of the material at the wavelength of the laser beam, λ_{th} is the heat conductivity, $\kappa_D = \lambda_{th} / (\rho \cdot c_p)$ represents the thermal conductivity, ρ is the mass density, and c_p is the specific heat capacity at constant pressure for the phase considered. The duration t_H for reaching a target temperature T_1 when starting from a given initial temperature T_0 on the surface of a material is therefore given by

$$t_H = \frac{\pi}{4} \cdot \frac{(T_1 - T_0)^2}{I^2} \cdot \frac{\lambda_{th} \cdot \rho \cdot c_p}{A^2}. \quad (2)$$

A select few values for κ_D and for $\lambda_{th} \cdot \rho \cdot c_p$, for a selection of common metals for the solid and liquid state, can be found in [27–31] and are summarized in Table A1.

For example, for aluminum in a liquid state at the melting temperature of $T_0 = 660^\circ\text{C}$, the time to reach a boiling temperature of $T_1 = T_V = 2520^\circ\text{C}$, when heating with an irradiance of $I = 5 \times 10^6 \text{ W/cm}^2$, is about 84 μs , corresponding to a frequency of about 12 kHz. The value of $\lambda_{th} \cdot \rho \cdot c_p = 2.8 \cdot 10^8 \text{ J}^2/\text{m}^4/\text{s}^1/\text{K}^2$ is taken for the liquid phase and the absorptivity of $A = 6\%$ for a laser wavelength of 1 μm . In comparison, in liquid iron at the melting temperature of $T_0 = 1540^\circ\text{C}$ with $\lambda_{th} \cdot \rho \cdot c_p = 1.8 \cdot 10^8 \text{ J}^2/\text{m}^4/\text{s}^1/\text{K}^2$ and $A = 40\%$, the time is about 0.6 μs , corresponding to a frequency of about 1.7 MHz, which is about $140\times$ higher.

2.2. Duration for Spreading the Heat

The thermal diffusion length $\ell_D = 2\sqrt{\kappa_D \cdot t_H}$ is commonly considered as a measure of the spatial extent of a temperature increase during the heating time t_H [1]. Solving for t_H gives the time

$$t_H = \frac{\ell_D^2}{4 \cdot \kappa_D} \quad (3)$$

it takes until a temperature increase reaches the extent ℓ_D . For the case of the semi-infinite body, which is uniformly heated on the surface, as considered before, the increase in the temperature at ℓ_D is about 9% of the temperature increase on the surface $T(0, t) - T_0$ after the heating time t_H [1].

For example, in solid iron, with $\kappa_{D,Fe} = 2.3 \times 10^{-5} \text{ m}^2/\text{s}$, the time for increasing the temperature to about 9% of $T(0, t_H)$ at the distance of 0.5 mm below the irradiated surface is about 2.8 ms, whereas in solid aluminum, with $\kappa_{D,Al} = 9.8 \times 10^{-5} \text{ m}^2/\text{s}$, this time is only about 640 μs , corresponding to frequencies of about 360 Hz and 1.6 kHz, respectively.

2.3. Propagation of Acoustic Excitations

The time for an acoustic excitation in a liquid metal to travel the distance d_w of the laser beam diameter on the workpiece is given by

$$t_S = d_w / c_S, \quad (4)$$

where c_S is the speed of sound. The values of which for liquid metals can be found in [29]. A few values for a selection of frequently used metals are summarized in Table A1.

For example, the time for an acoustic excitation to travel the distance of the diameter of a laser beam of 0.5 mm is about the same in aluminum and iron, $t_S = 0.1 \mu\text{s}$. It is noted that in deep-penetration laser welding, the length of the liquid zone in the direction of the material flow is much longer in steel than in aluminum and strongly depends on the processing parameters and beam shapes. Therefore, the time for an acoustic excitation to reach the solidification region must be calculated for each process parameter set.

2.4. Maximum Flow Speed Around a Keyhole

If a keyhole exists, e.g., during laser welding, the melt created in front of the keyhole must flow around the keyhole. The maximum velocity of this melt flow is one of the important quantities defining the quality of the weld, as was described in the introduction. An analytical approximation for the speed of the flow of the liquid metal around the keyhole is described in [1]. For a cylindrical keyhole with a diameter of the laser beam d_w and assuming that the velocity of the liquid metal v_L increases linearly from the border of the melt pool to the border of the keyhole, the maximum flow velocity $v_{L,max}$ can be approximated by

$$v_{L,max} = v_F \cdot \left(\frac{1}{\sqrt{10}} \left(\frac{T_V + T_L - 2T_0}{T_V - T_L} \right)^{\frac{5}{4}} \left(\frac{v_F \cdot d_w}{\kappa_T} \right)^{\frac{3}{4}} + 1 \right), \quad (5)$$

where v_F is the welding speed, T_L is the melting temperature, T_V is the vaporization temperature, and T_0 is the initial temperature. It can be seen that for low feed rates and small beam diameters, $v_{L,max} \approx v_{Feed}$, whereas for very high feed rates, the maximum flow velocity scales with about $v_{L,max} \propto v_{Feed}^{7/4}$. However, as the width of the liquid layer in Equation (5) is purely determined by heat conduction, it is possible to influence the maximum flow speed by increasing the difference between the lateral width of the melt pool and the lateral keyhole width, e.g., with modified laser beam profiles or beam wobbling.

The time for the liquid to pass the keyhole, within which it is possible to influence the melt flow with the laser beam, can be calculated with

$$t_{KH} = \frac{d_w}{v_{L,max}}. \quad (6)$$

Figure 1 shows the minimum liquid–keyhole–passing time as a function of the feed rate for aluminum (blue) and iron (orange) for a beam diameter of 0.5 mm and the material values $\kappa_{T,Al} = 9.8 \times 10^{-5} \text{ m}^2/\text{s}$ and $\kappa_{T,Fe} = 2.3 \times 10^{-5} \text{ m}^2/\text{s}$. At the feed rate of 6 m/min the keyhole-passing time for aluminum is about 10 ms and for steel 3 ms. At the feed rate of 60 m/min, the keyhole-passing time for aluminum is reduced to about 200 μs and for steel to 80 μs .

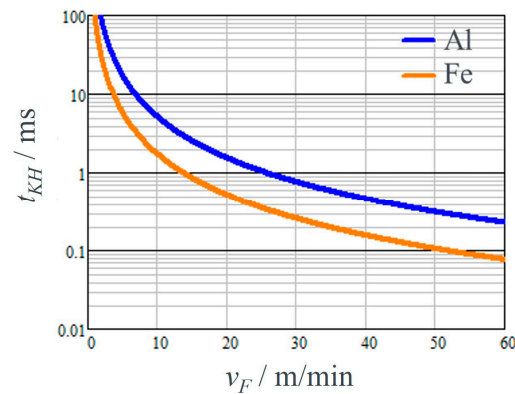


Figure 1. Minimum time for the liquid metal to pass the keyhole at its sides as a function of the feed rate v_F using Equations (5) and (6), calculated for aluminum (blue line) and steel (orange line).

2.5. Keyhole Response to Laser Excitation and Keyhole Collapse

Partial or complete keyhole collapse is the origin of several issues, such as blow outs or pore formation [1]. The keyhole collapse shows typical time constants t_c and quasi-periodicity with the frequency $f_c = 1/t_c$, which depends on the process parameters and the processed material. The time constants of the process are determined by convection in the melt pool and surface tension, as well as the evaporation rates within the keyhole, which determine how long it takes to open or close the keyhole in response to the laser beam being turned on and off or moved. Convenient analytical solutions do not exist to the best of our knowledge. However, recent publications allow for estimations of the time constants involved: the opening and closing time of a keyhole in steel was shown to be in the order of $t_c = 1$ ms [23], where it was observed that, in deep-penetration welding of steel, the tip of the capillary could clearly follow the movement of a laser beam, up to frequencies of $f_c = 100$ Hz, i.e., within about $t_c = 10$ ms, while no clear correlation to the excitation was found for frequencies of $f_{proc} = 1$ kHz and higher.

In contrast, the collapse of the tip of the keyhole can be much faster: in [32], megahertz X-ray imaging of an LPBF process with a $100\ \mu\text{m}$ laser beam in Ti revealed that the collapse at the tip of the keyhole, which might result in the formation of a pore, happened in about $t_c = 4\ \mu\text{s}$.

2.6. Summary of the Examples for Typical Time Constants and Frequencies

Table 1 shows a summary of a few typical process time constants for the physical quantities given above for a feed rate of 1 m/s and an average laser power of 10 kW. For the corresponding frequencies, a periodic repetition of the effect was assumed.

Table 1. Examples of a few typical process time constants and the respective frequencies for a feed rate of 1 m/s with an average laser power of 10 kW. A thermal diffusion length of $\ell_D = 0.5$ mm and a width of the laser beam on the surface of $d_W = 0.5$ mm was taken. T_L is the melting temperature and T_V the vaporization temperature of the respective material.

Effect	Material	Time (ms)	Frequency (kHz)
Heat conduction for $\ell_D = 0.5$ mm	Fe	2.8	0.4
Heat conduction $\ell_D = 0.5$ mm	Al	0.640	1.6
Temperature increase $T_L - T_V$	Fe	0.001	1000
Temperature increase $T_L - T_V$	Al	0.167	6
Sound wave $d_W = 0.5$ mm	Al/Fe	0.0001	10,000
Keyhole response to laser excitation	Fe	1	1
Keyhole collapse (for conditions, see text)	Ti	0.004	250

A thermal diffusion length of $\ell_D = 0.5$ mm and a width of the laser beam on the surface of $d_W = 0.5$ mm were taken as typical values. It can be observed that the frequency range spreads over more than four orders of magnitude, from the lowest frequencies in the range of 1 kHz to the highest frequency of 10 MHz. It can be assumed that characteristic frequencies of beam shaping are expected in this range. However, due to the strong dependence on the processing parameters and on the material properties, the values must be determined for each specific configuration.

3. Beam Shaping to Modify the Process: Basic Definitions

As described in the introduction, the literature describes a wide variety of approaches to beam shaping. However, the various methods are sometimes referred to by conflicting terms. We therefore propose consistent definitions for beam shaping and dynamic beam shaping below.

Beam shaping generally refers to any temporal and spatial manipulation of the beam shape, i.e., the laser beam's spatio-temporal intensity distribution $I(x, y, z, t)$ and its polarization. This begins within the laser resonator, where the beam is generated as a superposition of resonator modes. Temporal properties such as repetition rate and pulse shape are defined by techniques like mode locking or Q-switching. Extra cavity spatial beam shaping includes all approaches reviewed in [19–21], as well as power modulation and pulse stretching or compression. Hence, beam shaping—as the term implies—refers solely to the manipulation of the beam itself.

The primary goal in laser applications, however, is not merely to shape the beam but also to achieve process modifications that enhance process quality and productivity. The actual impact on the process is governed by the irradiance distribution $J(x, y, z, t)$ and the polarization on the surface of the workpiece. In the simplest case of a beam incident on a flat surface, the irradiance is given by $J(x, y, z, t) = \cos(\varphi)I(x, y, z, t)$, where φ is the angle of incidence and I is the intensity distribution in the cross-section of the beam. In most practical scenarios, however, the irradiance at the workpiece—and therefore the spatio-temporal distribution of the absorbed power density—is influenced by the geometry of the interaction zone and by multiple reflections therein. The geometry might change dynamically, leading to a time-dependent absorbed power density. As a result, the locally absorbed irradiance is determined by both the beam shaping and the process conditions, and these two aspects cannot be considered independently. This means that the process modifications cannot be directly related to the beam shapes, making deterministic process design very challenging.

In the following, consistent terms involved in “beam shaping” and “dynamic beam shaping” and the resulting process modifications are proposed in view of their temporal characteristics. The aim is to suggest a general convention for a nomenclature to facilitate comparison across the wide range of methods that use beam shaping to influence laser processes and also to enable an unambiguous exchange between different disciplines, like optics, systems engineering, materials processing, or manufacturing.

For the case of laser material processing considered here, the process parameters are referred to as χ in the following. This includes quantities such as material properties, feed rate, laser power, focus position, and irradiance distribution. For easier distinction, process parameters related to beam shaping are referred to as χ_B .

In contrast ψ refers to all process features such as the width and depth of a weld seam, the diameter and depth of a keyhole, the width of a heat-affected zone, the velocity of the melt flow, spattering, and pore formation. In practice, the process parameters χ are optimized and adjusted to achieve specific desired process features ψ , which are optimal for a specific application. In the following, the considerations are focused on the process

itself, i.e., we consider the interaction zone through which the material moves depending on the feed rate. This perspective aligns with the energy, momentum, and force balances that govern process stability.

3.1. Static Process Modifications

Most laser-based processes achieve optimum quality when operating in a form of dynamic steady state. In the simplest case, this state is achieved with static process modifications, i.e., time-invariant process parameters with $\dot{\chi} = 0$. This includes, for example, a constant relative velocity $|\vec{v}|$ between the laser beam and the workpiece along a linear path, where $\dot{\vec{v}} = 0$. A steady state can also be maintained during motion along a circular path, provided the relative speed remains constant. In this case, $\vec{v} \cdot \dot{\vec{v}} = 0$, while $\dot{\vec{v}} \neq 0$, due to the continuous change in direction. In both scenarios, the absence of wobbling is essential for maintaining a constant absolute value $|\vec{v}|$ of the speed.

Static beam shaping, therefore, refers to measures that aim at adjusting the intensity distribution $I(x, y, z)$ and the polarization of a beam permanently and constantly, i.e., with no temporal change, with the goal to reach static process modifications, which optimize the specific process features. This is reported in [4], where the two process features spatters and pores are minimized with superimposed laser beams. In [25], a beam with a core and ring profile enabled smooth and pore-free deep penetration welds with a subsequent wire filling process in brass. In [26], a mm wide annular beam shape enabled control of the melt pool to reduce process defects.

3.2. Dynamic Process Modifications

The term “dynamic process modification” in the following refers to methods in which one or more process parameters, $\chi = \chi(t)$, vary over time. This is characterized by $\dot{\chi} \neq 0$ and/or $\vec{v} \cdot \dot{\vec{v}} \neq 0$. The variation in the process parameters might occur during the modulation time t_χ or with the modulation frequency f_χ .

3.2.1. Characteristic Time Constants and Characteristic Frequencies

Laser processing with varying process parameters that change during a time t_χ in a non-periodic manner, is the state of the art in laser cutting, where usually the average laser power is adapted to the current feed rate at the beginning of a cut or during cutting of corners to keep the line energy constant. The duration, over which the laser power is decreased or increased, is adapted to the geometry of the cut, the feed rate and the acceleration. Further examples are the adaptation of the focal position and the laser power to changes in the thickness of the material. Such parameter modulations have characteristic time constants, which are given by properties of the processing system, the material properties of the processed sample and properties of the process itself.

The focus in this paper is on periodic parameter changes with frequencies f_χ that are inherent to DBLs. It is seen that with periodic parameter changes, characteristic modulation frequencies exist at which the influence on the process is particularly strong, as described in the introduction. More generally speaking, it is observed that some of the features ψ of a process are sensitive to the frequency of periodic changes in specific process parameters χ , i.e., that a process feature ψ undergoes pronounced changes when a process parameter χ is modulated at a certain characteristic frequency ${}^\psi_\chi f_i$, where $i = 1, 2, 3 \dots$ takes into account that there may be several different characteristic frequencies at which the process feature ψ is sensitive to a modulation of χ . The types of dynamic process modifications are discussed in the following.

3.2.2. Non-Periodic Dynamic Process Modifications

With non-periodic process modifications, one or more parameters are changed as a function of time during the process, where t_M is the duration of the non-periodic modification. The best process result is obtained when non-periodic dynamic process modifications are adapted to the characteristic time constants involved in the process, as described in the previous section.

3.2.3. Periodic Dynamic Process Modifications

With periodic dynamic process modifications, one or more process parameters are changed in a periodic manner during the process, i.e., with the frequency f_χ . For periodic process modifications, it is therefore more expedient to use frequencies than times. It is noted that periodic process modifications are usually addressed when considering Civan's DBLs, which are used as an example in this paper. With these lasers, both the positioning of the beam within a shape and changing between shapes can be done with a selectable frequency. The parameter modifications, which are induced with this dynamic beam shaping, must be compared to the characteristic frequencies involved in the considered process. This comparison leads to the three distinct regimes discussed in the following.

Direct Periodic Process Modifications

When a process parameter χ is periodically changed with a frequency $f_\chi \ll \min(\psi_\chi f_i | \forall i)$ that is much smaller than any of the characteristic frequencies, the feature ψ directly follows the variation in the parameter $\chi(t)$ as the process at any time t continuously but momentarily adopts the state that would be obtained with the current value of $\chi = \chi(t)$ in a static process modification.

Characteristic Periodic Process Modifications

A process feature ψ is subject to characteristic peculiarities when the modulation frequency $f_\chi \approx \psi_\chi f_i$ of the process parameter χ lies within a more or less large range around the characteristic frequency $\psi_\chi f_i$ defined above.

It is important to note that the modulation of process parameters with a characteristic frequency $\psi_\chi f_i$, may be at resonance with typical process frequencies, at which a given feature tends to respond with a disproportionally strong amplitude to the excitation, or at antiresonance, at which the response of a process feature is disproportionally small, or at any other frequency, leading to a characteristic behavior. Depending on the damping, there is always a certain bandwidth around these frequencies within which the features respond in the characteristic manner. Knowledge of the characteristic process frequencies is therefore the key to deterministic process modification.

Although this is the most challenging regime for process modifications, it has a large potential for inducing very strong modifications of the process.

Quasi-Static Periodic Process Modifications

When the process parameter χ is periodically changed with a frequency $f_\chi \gg \max(\psi_\chi f_i | \forall i)$ that is much higher than any of the characteristic frequencies, the process features cannot follow the immediate changes in the process parameters. Therefore, it will typically adopt a state that corresponds to the one obtained with a quasi-static value of $\bar{\chi}$ that equals the time average of $\chi(t)$.

3.2.4. Periodic Dynamic Beam Shaping

Periodic dynamic beam shaping refers to all beam shaping approaches that generate a periodic temporal change in the intensity and polarization distribution in the beam

reaching the interaction zone of the process, which leads to the periodic dynamic parameter modifications χ_B with the frequency f_{χ_B} . This includes methods such as beam wobbling, periodic modulation of the average power, very fast repositioning of a laser beam on the surface to generate a time-averaged intensity distribution, and periodic modulation of the beam shape, as is of particular interest with DBLs. In this case, the intensity distribution reaching the workpiece may be simultaneously characterized by several frequencies f_{χ_B} related to different parameters χ_B involved in the dynamic beam shaping methods applied. These may include wobbling frequency, power modulation frequency, or the shape refresh and shape switch frequency of DBLs. It is important to emphasize that the term “dynamic” here refers to the way in which beam shaping is performed and is independent of the properties of the process. Whether periodic dynamic beam shaping acts as a direct, characteristic, or quasi-static dynamic process modification depends on the comparison with the characteristic frequencies $\psi_{\chi} f_i$ as described above. The relations, which define the processing regimes, are summarized in Table 2.

Table 2. Summary of the regimes of dynamic process modifications induced by periodic dynamic beam shaping.

Regime of Periodic Process Modifications	Condition
Direct process modification of feature ψ	$f_{\chi_B} \ll \min(\psi_{\chi} f_i \forall i)$
Characteristic process modification of feature ψ	$f_{\chi_B} \approx \psi_{\chi} f_i$
Quasi-static process modification of feature ψ	$f_{\chi_B} \gg \max(\psi_{\chi} f_i \forall i), \forall b$

To clearly distinguish between the regimes, the two operators “ \ll ” and “ \gg ” are recommended. Note that it is possible that a process is simultaneously influenced in different regimes of different parameters.

4. Summary of Properties and Frequency Definitions of DBLs

To clarify the understanding of the definitions in the previous section, examples for periodic process modifications based on the properties of Civan’s Dynamic Beam Laser (DBL) are given in the following. This laser can modify process parameters χ periodically with frequencies f_{χ} of up to 80 MHz. This is higher than any of the frequencies listed in Table 1, making process modifications possible in all three regimes. The properties of the current Civan DBLs are extensively described in [33]. However, the basic properties are summarized in the following to ease the reading of this paper.

4.1. Properties of Points

Coherent combining of a bundle of fundamental-mode fiber lasers allows for the generation of a plane overall phase front, which results in a “point”—more precisely, a diffraction pattern with a main lobe with high intensity—in the focal plane of a focusing lens. This main lobe contains up to 60% of the total laser power and is almost diffraction-limited. The diameter of the main lobe depends on the focal length of the focusing lens. Figure 2a shows a false-color representation of the calculated, normalized intensity distribution for a main lobe created with a bundle of 36 fiber lasers, which is set in the center of the blue square (marked with the blue arrow). The color scale is shown on the right of Figure 2a. The blue square represents the active area that contains >99.9% of the total laser power. Small side lobes to this main lobe appear in the active area, because the combined fibers represent a structure of a diffraction grating. By tilting the common phase front, the point can be set at arbitrary positions (x, y) as shown in Figure 2b. It can be observed that the side lobes move with the main lobe, and that the relative height of some of the peaks of the

diffraction pattern is increased. The point can be set within the maximum positions (x_{min} , x_{max}) and (y_{min} , y_{max}) that are given by the position, where the relative height of the main lobe and the three accompanying side lobes is the same as shown in Figure 2c. The distance $x_{max} - x_{min} = y_{max} - y_{min} = d_S$ is referred to as the scan width. The width of the blue area is the active area, which is about $3 \times$ the width of the area within which the points can be set. The height of all lobes varies with the position in this area. Details are given in [33].

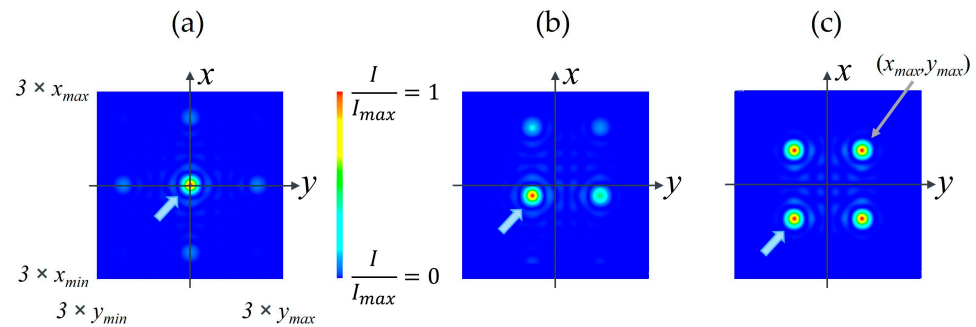


Figure 2. (a) Main lobe (i.e., “point”, marked with the blue arrow) set in the center of the active area and the accompanying weak diffraction pattern; (b) point set at an arbitrary position (x , y); (c) point set at the position (x_{max} , y_{max}) where the main lobe and all diffraction lobes have the same maximum intensity.

The following Table 3 lists typical values for the diameter of the main lobe, d_{ML} , the resulting maximum intensity for a 12 kW-laser, $I_{max,0,0}$, and the diameter of the active area, $d_{ActiveArea}$, for different focal lengths of the focusing lens f_L .

Table 3. Diameter of the main lobe d_{ML} , maximum intensity in the center $I_{max,0,0}$, scan width d_S , and width of the active area $d_{ActiveArea}$ for a few focal lengths of the focusing lens, f_L , and a DBL with 12 kW of output power.

f_L (m)	d_{ML} (μm)	$I_{max,0,0}$ (W/cm^2)	d_S (μm)	$d_{ActiveArea}$ (μm)
0.75	68	4.0×10^8	129	709
1.0	91	2.2×10^8	172	945
1.5	136	9.9×10^7	258	1418
3.0	272	2.5×10^7	516	2836

It is noted that the maximum intensity is only reached when the point is set in the center of the active area with $x = y = 0$. At the positions (x_{max} , y_{max}), where the main lobe and the side lobes have the same height, the maximum intensity equals about 54% of $I_{max,0,0}$.

4.2. Sequences of Points Create Shapes

The adjustment of the phases of the combined fibers is made with electro-optic modulators (EOMs) in Civan’s DBL. The EOMs are operated at a maximum frequency of $f_{max} = 80$ Mhz, and therefore, allow for the creation of a common phase front, and with it a point within $t_{min} = 12.5$ ns. This is a much shorter time constant than any encountered in laser processes as described in Section 3. Therefore, it is possible to create arbitrary, quasi-static shapes composed by a very fast sequence of N_{SP} points, which can be set at N_{Pos} arbitrary positions. A position of a point in the shape can be addressed more than once. On the one hand, this increases the total number of points in the shape, N_{SP} . On the other hand, it increases the locally deposited energy compared to the other shape positions

with fewer points per position. It is noted that increasing the number of points per position increases the fluence at this position but not the intensity.

The shape refresh frequency, i.e., the frequency with which the complete shape is redrawn, f_{SR} , can be chosen arbitrarily. This refresh frequency defines the point-frequency, which is given by $f_{SP} = f_{SR} \cdot N_{SP}$, with the boundary condition that $f_{SP} \leq f_{max}$. In fact, it is recommended to keep f_{SP} smaller than about 50% of f_{max} to ensure clean build-up of every single point in the shape. Figure 3 shows a selection of quasi-static shapes. N_{SP} equals the total number of points in the shape. Figure 3a shows a square with nine shape positions, $N_{Pos} = 9$. Each position was addressed with one single point once, therefore $N_{SP} = 9$. Figure 3b shows the same square, with $N_{Pos} = 9$, but the central position (index $i = 5$) was addressed three times ($n_{SP,i} = 3$), resulting in $N_{SP} = 11$. The spiral and the hourglass, shown in Figure 3c,d, respectively, show the capability of DBLs to generate complex average shapes. These two shapes might be used, for example, to widen a keyhole because it generates a larger quasi-static shape, while the maximum intensity at each position in the shape remains almost constant, because the intensity of the points in the sequence does not change significantly in the active area. This allows for keeping the intensity at each point high enough to stay above the deep penetration threshold [1].

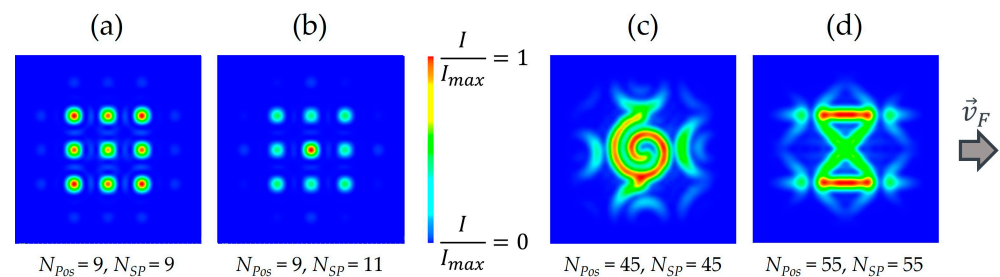


Figure 3. Examples for shapes created with a sequence of points. N_{Pos} is the number of addressed positions used for creating this shape, N_{SP} is the total number of sequentially addressed single points. (a) shows the resulting shape with 9 points at 9 different positions, while in (b) the center point was placed three times, resulting in 11 points at 9 positions. The spiral and the hourglass shown in (c) and (d), respectively, might be used, for example, to widen a keyhole. The feed direction is to the right. The scale of the false-color images is the same as in Figure 2.

Apart from creating single shapes, DBLs have the capability to switch between shapes, i.e., creating sequences of shapes. The switching can be done at very high frequencies, only limited by the condition $f_{SP} < f_{max}$, which must hold for each shape in the sequence. Switching between the shapes can either be done periodically, with the shape duration frequency f_{SD} , or non-periodically, where every shape in the shape sequence has its own shape duration. The latter case adds additional complexity to dynamic beam shaping and is not considered in the following.

The capability of switching shapes was demonstrated in several experiments: triangles with opposite orientation have been used to demonstrate the completely different influence of the two shapes on the hydrodynamic behavior in liquid iron [34], and switching between a single point in the center of the active area and a curved line perpendicular to the feed direction allowed for pore-free welding of thick mild steel, as described in [34].

Furthermore, DBLs allow for actively shifting the focus position in the direction of beam propagation by creating a parabolic common phase front. This can also be done in 12.5 ns. Details regarding shape sequences and active focus shift (referred to as focus steering) are given in [33].

5. Deterministic Approach for Solutions to Process Issues Using DBLs

The preceding section shows that DBLs offer a very wide range of possible beam shapes and modulation frequencies. This makes it difficult to find solutions for specific tasks through trial and error. Therefore, this section proposes a deterministic approach to identify promising beam shapes and frequencies. As an illustrative example, the emerging of process pores during the welding of AlMg with an average laser power of 3.4 kW, a laser focus diameter of 680 μm , and a feed rate of 4 m/min is used.

5.1. First Step: Identify Possible Cause

The first step is to analyze possible mechanisms that cause the process issue. This requires a basic understanding of how the process issues develop. The mechanism for the illustrative example of the formation of a process pore is described in Figure 4a–e, which shows a sequence of six images, taken out of an X-ray film, with a total duration of about 15 ms. The X-ray film was recorded with a frame rate of 2 kHz. The bright areas with the dashed, white border represent the keyhole, and in addition, in (Figure 4d), a bubble and, in (Figure 4e), a pore. It is seen in (Figure 4a) that the starting point for the formation of a pore is a straight, narrow keyhole, which starts to bulge (Figure 4b) and then, in (Figure 4c), constricts (red arrow) due to the fast vapor flow out of the keyhole and the corresponding Bernoulli effect, which decreases the pressure in the upper part of the keyhole. Just before the collapse, the tip of the keyhole is shaded against the laser beam, and the vapor in the keyhole condensates on its surface, resulting in an underpressure, which sucks ambient air or process gas into the keyhole. After the collapse (red arrow), a gas-filled bubble remains, which results in a pore when the material is solidified (Figure 4d). The narrow keyhole is building up again (Figure 4e), finally restarting the cycle with a straight, narrow keyhole (Figure 4f).

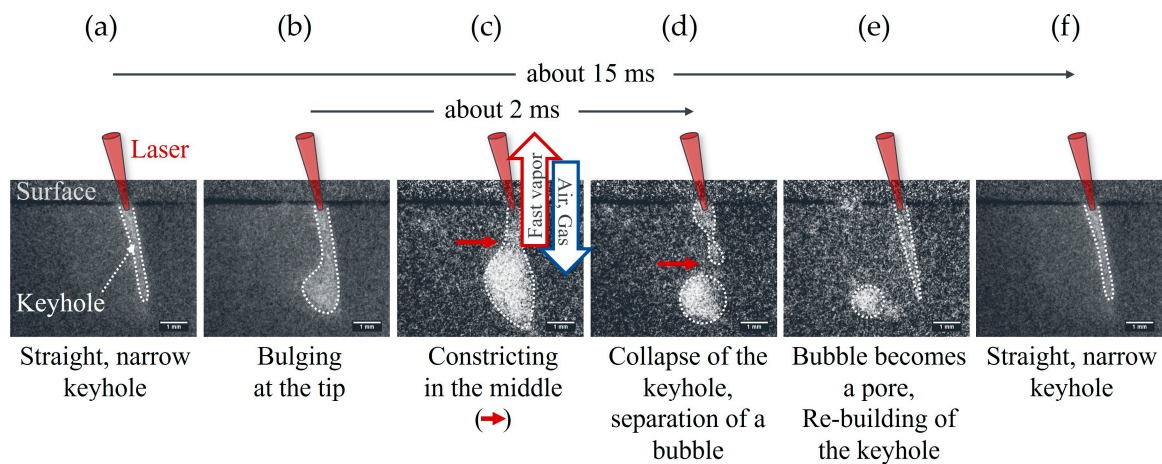


Figure 4. (a–f) Sequence of five X-ray images with a total duration of about 250 μs describing the formation of a process pore during welding of AlMg with an average laser power of 3.4 kW and a feed rate of 4 m/min. The details are described in the text.

For the parameters investigated here, the duration for a complete cycle is in the range of 15 ms, yielding a characteristic frequency $f_{\psi,1} \approx 70$ Hz. The duration for bulging, constricting and separation of a bubble is about 2 ms, yielding a characteristic frequency $f_{\psi,2} \approx 500$ Hz.

5.2. Second Step: Identify Possible Solutions

The second step is to evaluate possible beam shapes that can be used to solve the issue. In the example of process pore formation, the narrow keyhole, shown in Figure 4a,f, is

the starting point of the cycle. Therefore, widening the keyhole and keeping it open is a promising approach for reducing the number of pores.

5.3. Third Step: Identify Possible Beam Shapes and Frequencies

The use of a spiral or an hourglass, as shown in Figure 3c,d, as the beam shape is a straightforward approach. The maximum intensity in the beam must be chosen to exceed the deep penetration threshold for a moving beam as described in [1]. This is done by the proper selection of the focal length of the focusing lens and the laser power. Furthermore, the diameter of the spiral must be chosen large enough to prevent the bulging and constricting shown in Figure 4b,c. The pictures in Figure 4 suggest that the diameter of the keyhole at the entrance, and therefore the diameter of the shape, should be about three times larger than the diameter of the focus. Possible values for these beam parameters can be estimated from the numbers listed in Table 3 or calculated with the formula given in [33].

5.4. Fourth Step: Determine the Characteristic Frequencies

Possible characteristic frequencies for the desired process feature, given the process parameters and the material being processed, can be estimated from the physical quantities in Section 2. However, a definitive determination must usually be made experimentally. In this example, two typical frequencies of 67 Hz and 500 Hz can be determined from the X-ray imaging. It is noted that the X-ray film was taken with a frame rate of 2 kHz, and therefore, no effects with higher frequencies than this could be detected. A more practical example of how to determine characteristic frequencies experimentally is described in detail in Section 6.

5.5. Fifth Step: Deterministic Approach for Selecting Frequencies to Correct Process Issues

The four steps described in the preceding sections are summarized in Table 4. The first two columns show the possible physical approach and promising shapes. The third column summarizes the characteristic frequencies $\psi_\chi f_i$. In the present example, the process feature ψ is the formation of pores. For the process parameter χ , the dynamic beam shape is taken, which is refreshed with the characteristic frequency $\psi_\chi f_1 = 70$ Hz and $\psi_\chi f_2 = 500$ Hz. In the case of Civan's DBLs, each of the three regimes, direct, characteristic and quasi-static, as defined in Table 2, has to be considered for both the shape refresh frequency f_{SR} and the shape duration frequency f_{SD} , as defined before. The operators " \ll " and " \gg " are taken to be one order of magnitude for this example to be in accordance with the "one decade rule" in classical control theory, ensuring sufficient frequency separation between cascaded control loops or between a system's bandwidth and its resonant/disturbance frequencies. The green values in the table finally propose meaningful frequencies f_{SR} and f_{SD} for testing with the process. When changing the frequencies, $f_{SP} \leq f_{max}$ must be considered.

It is noted that the numbers in green result from the evaluation of the X-ray film, which does not allow for the consideration of frequencies larger than 2 kHz. However, these numbers may be taken as starting points for experimental investigations on how to reduce process pores during welding of AlMg with an average laser power of 3.4 kW, a laser focus diameter of 680 μm , and a feed rate of 4 m/min. The determination of characteristic frequencies with X-ray technology was helpful to explain the methodology behind the deterministic approach for selecting frequencies to correct process issues. Usually, it is much simpler and purposeful to determine characteristic frequencies with the process itself. An example of doing this is given in the following.

Table 4. An example of a deterministic approach for selecting frequencies to reduce the formation of process pores, as well as summaries of the possible frequency regimes for the periodic dynamic process modifications.

ψ is the Emergence of Pores			Direct		Characteristic		Quasi-Static	
Approach	Shape(s) χ	ψ_{f_i}	Shape Refresh $f_{SR} \ll \psi_{f_i}$	Shape Duration $f_{SD} \ll \psi_{f_i}$	Shape Refresh $f_{SR} \approx \psi_{f_i}$	Shape Seq. $f_{SD} \approx \psi_{f_i}$	Shape Refresh $f_{SR} \gg \psi_{f_i}$	Shape Seq. $f_{SD} \gg \psi_{f_i}$
Widen keyhole	Spiral or Hourglass	70 Hz	$f_{SR} \leq 7 \text{ Hz}$	$f_{SD} \leq 7 \text{ Hz}$ $f_{SR} \geq 700 \text{ Hz}$	$f_{SR} \approx 70 \text{ Hz}$	$f_{SD} \approx 70 \text{ Hz}$ $f_{SR} \geq 700 \text{ Hz}$	$f_{SR} \geq 700 \text{ Hz}$	$f_{SD} \geq 700 \text{ Hz}$ $f_{SR} \geq 7 \text{ kHz}$
Widen keyhole	Spiral or Hourglass	500 Hz	$f_{SR} \leq 50 \text{ Hz}$	$f_{SD} \leq 50 \text{ Hz}$ $f_{SR} \geq 5 \text{ kHz}$	$f_{SR} \approx 500 \text{ Hz}$	$f_{SD} \approx 500 \text{ Hz}$ $f_{SR} \geq 5 \text{ kHz}$	$f_{SR} \geq 5 \text{ kHz}$	$f_{SD} \geq 5 \text{ kHz}$ $f_{SR} \geq 50 \text{ kHz}$

6. Experimental Verification of the Process Regimes

Experimental verification of the varying effects of the periodic modification of process parameters χ with frequencies f_χ in the three process regimes was achieved with the example of welding of die cast aluminum with a thickness of 2 mm. This process usually suffers from many pores and is therefore useful for analyzing the influence of dynamic beam shaping. The emergence of pores, therefore, represents the process feature ψ in this example. For the experiments, a DBL-14 kW laser creating a “spiral” beam shape (Figure 5a) consisting of 45 points, as shown in Figure 3c, was chosen. Since the spiral is not symmetrical, the shape refresh frequency influences the process, even though the shape was not changed in a sequence. The laser power was set to 2.8 kW and the feed rate to 200 mm/s. The focal length of the focusing lens of 1 m yielded a diameter of a single point in the shape of 91 μm ; the spiral had a diameter of about 610 μm . Argon was used as a shielding gas with a flow rate of 30 L/min. For the experiment, the shape refresh frequency f_{SR} was changed from 10 kHz up to 500 kHz, resulting in a point frequency f_{SP} of 500 kHz and 22.5 MHz, respectively. The shape duration was set longer than the duration of the complete weld. The shape refresh frequency represents the periodic dynamic parameter modification χ_B with the frequency $f_{\chi_B} = f_{SR}$.

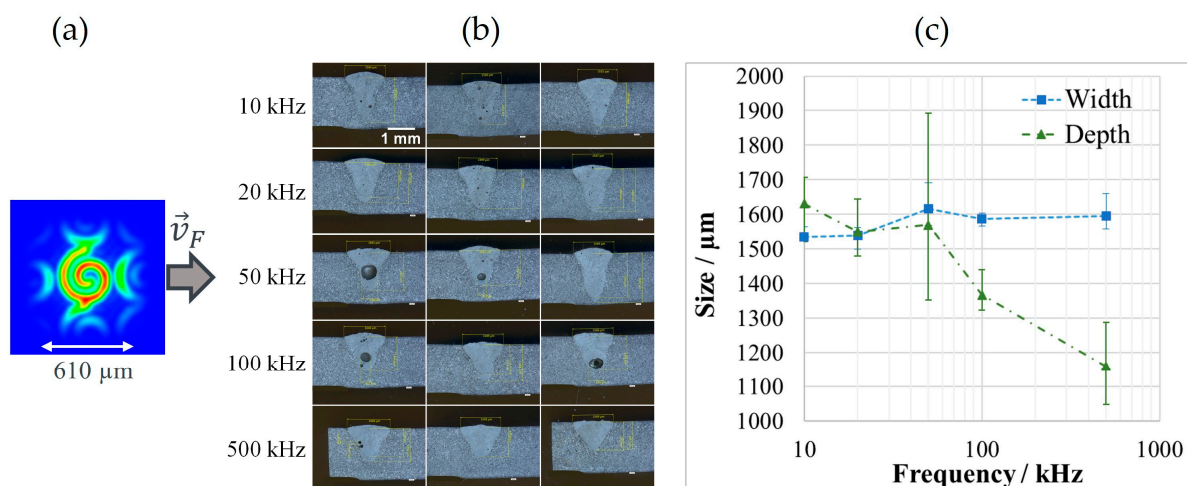


Figure 5. (a) Spiral beam shape with 45 points (as described in Figure 3c) used for the experiments. The feed direction is to the right. (b) Cross-sections of the welds in cast aluminum for the five different shape refresh frequencies. (c) Width (blue rectangles connected with dashed lines) and depth (green triangles connected with dash-dotted lines) of the welds. The error bars indicate minimum and maximum values measured in the three experiments.

The processed aluminum die-cast specimens were sectioned using Struers Labotom-5 and Secotom-6 cutting machines and subsequently embedded in VersoCit-2 acrylic resin.

Polishing was performed on a Struers LaboPol-30 system equipped with a LaboForce-100 head, accommodating up to six 30 mm or three 50 mm mounted samples. The procedure followed the standard Struers methodology with minor adjustments to polishing duration according to sample size. For routine specimens, the final MD-Chem polishing step was omitted. Etching was conducted using Keller's reagent (190 mL distilled water, 5 mL HNO₃ 70%, 3 mL HCl 32%, and 2 mL HF 48%), applied by dripping the solution onto the surface with a pipette, followed by rinsing with distilled water. The welded samples were examined under a microscope with an objective of X5 to image the cross-section. The microscope was connected to a camera that provides an additional X10 magnification. The percentage of porosity in the welds was manually determined using the ImageJ v1.54-software, following a consistent image analysis procedure: The image to analyze was imported into the software and converted into 8-bit grayscale. Using "Image" → "Adjust" → "Threshold", the threshold settings were adjusted to ensure that the pores in the image were correctly highlighted in red. If the pores were not accurately captured, the threshold levels were manually fine-tuned to improve detection. A freehand selection tool was then used to define the specific weld area for analysis. Finally, by selecting "Analyze" → "Measure", the software generated a results window displaying the percentage area, which corresponds to the porosity percentage within the selected weld region. This technique allows for the measurement of pores with diameters down to a few microns.

Figure 5b shows the cross-sections of the welds for the five different shape refresh frequencies. Three identical experiments were made for each shape refresh frequency. Figure 5c shows the width (blue rectangles connected with dashed lines) and the depth (green triangles connected with dash-dotted lines) of the welds as a function of the shape refresh frequency. The error bars indicate the minimum and maximum values measured in the three experiments. It can be seen that the width of the weld seams remains constant at about 1600 µm at all frequencies. In contrast, the depth remains only constant up to 50 kHz, also at about 1600 µm. At 100 kHz, the depth decreases by about 15% to 1370 µm, and, at 500 kHz, it decreases by almost 30% to 1160 µm. This indicates that for shape frequencies exceeding 50 kHz, the process becomes less efficient. A straightforward explanation is that at the lower frequencies, the shape of the keyhole, and with it the efficiency of the incoupling of the laser beam [1], is determined by the dimensions of the small, single, moving main lobe, while for the higher frequencies, the shape of the keyhole is mainly determined by the large, average shape of the spiral.

Figure 6 shows the porosity in percent of the welding cross-section as a function of the shape refresh frequency. The error bars correspond to the minimum and maximum values of the measured porosity. The measured porosity clearly allows for the interpretation of the three process regimes summarized in Table 2.

At the shape refresh frequencies of 50 kHz and 100 kHz, the average porosity is significantly increased. This corresponds to the transition of the process, as can be observed in Figure 5c. Furthermore, the large error bars indicate a strong influence of the modulation frequency. It can therefore be concluded that a characteristic frequency for the process feature pore formation in cast aluminum at the feed rate of 0.2 m/s and an average laser power of 2.8 kW is $\psi f_1 = 75 \pm 25$ kHz. At low frequencies with $f_{\chi B} = f_{SR} \ll \psi f_1$, the process modifications are therefore in the direct frequency regime and at high frequencies with $f_{\chi B} = f_{SR} \gg \psi f_1$ in the quasi-static frequency regime. In the present example, it is clearly seen that direct process modulation at $f_{SR} \approx 20$ kHz and quasi-static process modulation at $f_{SR} \approx 500$ kHz are favorable. The direct process modulation with $f_{SR} \approx 20$ kHz has the additional advantage of relatively small error bars.

It is straightforward to interpret that the relatively slowly moving keyhole allows pores to outgas and to collapse, as observed for conventional beam oscillation in [14].

However, it is noted that the frequency seen in the present experiment is high compared to both the frequency seen in [14] and the frequency determined in the example in the previous section for the growth of process pores. This suggests that the mechanism of pore formation in cast aluminum is completely different.

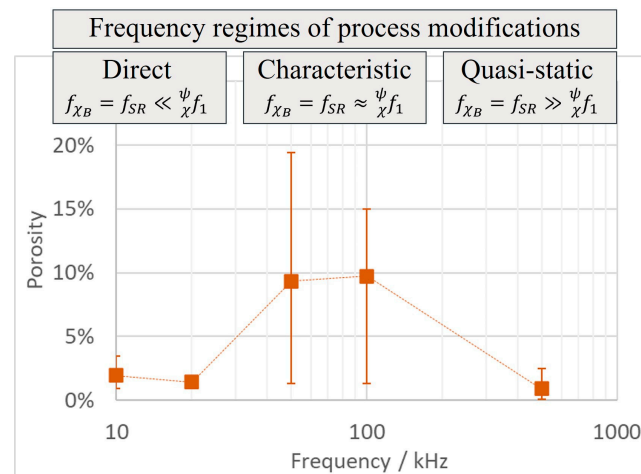


Figure 6. Process feature ψ = porosity in percent of the welding cross-section as a function of the shape refresh frequency f_{SR} , which is the periodic dynamic parameter modification χ_B with the frequency f_{χ_B} in this example. The labels above indicate the three identified frequency regimes of process modifications.

The characteristic frequency obtained in Figure 6 can be used to define the table with the deterministic approach for selecting frequencies to correct process issues. This is of particular interest if other beam shapes should be tested or the welding of different cast materials should be optimized.

The following considerations might help to apply the obtained result to other process parameters: The duration for moving the diameter of the spiral of 610 μm at the feed rate of 0.2 m/s is 3 ms. Therefore, the spiral is drawn 60 times at the shape refresh frequency of 20 kHz, and the spiral is moving 10 μm , while it is being drawn once. This is about 9% of the diameter of the main lobe of 91 μm . It can be assumed that the value of 9% should be taken as a reference if, e.g., the feed rate is to be increased. This can be done by either increasing the diameter of the spiral using a longer focal length lens or by increasing the shape refresh frequency. In addition, the laser power must be increased to stay in the same regime with respect to the deep penetration threshold following [1].

Finally, it is noted that a priori, there is no “good” or “bad”; there exist just different modulation regimes, which must be systematically and experimentally determined to find the best regime.

7. Conclusions

Dynamic beam shaping offers a novel and very large field for active process modifications for laser applications. With dynamic beam lasers (DBLs), this can be done by creating specific beam shapes or even by fast switching between different beam shapes. Clear improvements are described in [34], where switching between a single point in the center of the active area and a curved line perpendicular to the feed direction allowed pore-free welding of very thick mild steel. However, the basic principle of DBLs is to create shapes as a sequence of points, which can be generated at an arbitrary position in the focal plane with frequencies up to 80 MHz. Each shape has, therefore, a refresh frequency, with which the complete shape is drawn. Furthermore, switching between the shapes introduces an

additional frequency. Therefore, finding the optimum beam shaping method for successful process modifications is very challenging.

The basis of the present study is to relate the frequencies involved in dynamic beam shaping to the characteristic frequencies observed in dynamic process modifications. From experimental results, e.g., as described in [24], it is seen that dynamic process modifications feature characteristic frequencies, where the influence on a process feature, such as the formation of pores or spatters, is particularly strong.

Definitions of the nomenclature of the relation between the frequencies resulting from dynamic beam shaping with DBLs and the characteristic frequencies observed separate dynamic periodic process modifications in the three distinct frequency regimes: direct, characteristic and quasi-static, where the beam shaping frequency is much lower, about the same, or much higher than the characteristic frequency, respectively. The characteristic frequencies depend not only on the laser process and the process feature under consideration, but also on the material being processed and the specific processing parameter settings. Therefore, the range of characteristic frequencies can vary by several orders of magnitude. This becomes clear in Section 2, where the time constants of typical physical quantities are described, as well as in the examples in Sections 5 and 6, where the characteristic frequencies for the formation of process pores in AlMg and the porosity in cast aluminum differ by almost four orders of magnitude. However, knowledge of the characteristic frequencies is necessary for deterministic process design with dynamic beam shaping. Therefore, these frequencies should be determined experimentally for each process for the desired process features.

The experimental example of influencing the porosity during welding cast aluminum described in Section 6 validates the occurrence of a characteristic frequency and the three significantly different process regimes, and with it, the need for a systematic approach as described in this paper.

Author Contributions: Conceptualization, R.W., R.A. and A.S.; methodology, R.W., K.G. and T.G.; validation, T.G., K.G., C.H., R.A., E.G. and N.A.; formal analysis, R.W., T.G., C.H., R.A., E.G. and N.A.; investigation, R.A., E.G. and N.A.; resources, E.S. and A.S.; data curation, R.W. and R.A.; writing—original draft preparation, R.W.; writing—review and editing, R.W., T.G., K.G., C.H., A.S., E.S., R.A., E.G. and N.A.; visualization, R.W.; supervision, E.S. and T.G.; project administration, R.W. and A.S.; funding acquisition, E.S. All authors have read and agreed to the published version of the manuscript.

Funding: This research received no external funding.

Data Availability Statement: Data will be made available upon request to interested researchers.

Conflicts of Interest: Authors Ami Spira, Nina Armon, Ehud Greenberg, Rachel Assa and Eyal Shekel were employed by the company Civan Advanced Technologies. The remaining authors declare that the research was conducted in the absence of any commercial or financial relationships that could be construed as a potential conflict of interest.

Abbreviations

The following abbreviations are used in this manuscript:

IFSW	Institut für Strahlwerkzeuge, University of Stuttgart
DED	Wire-based material deposition/directed energy deposition
PBF-LB	Powder bed fusion by a laser beam
DBLs	Dynamic beam lasers
LPBF	Laser powder bed fusion

Appendix A

Selection of Material Constants

Table A1 summarizes thermal constants taken from [27,28] and speed of sound in liquids, c_s , taken from [28–31], for a selection of common metals, with $\kappa_D = \lambda_{th} / (\rho \cdot c_p)$ and $\kappa_T = \rho \cdot c_p \cdot \lambda_{th}$, where λ_{th} is the heat conductivity, ρ is the density, and c_p is the specific heat capacity at constant pressure.

Table A1. Thermal constants and speed of sound for a selection of common metals.

Metal	κ_D Solid (m ² /s)	$\lambda_{th} \cdot \rho \cdot c_p$ Solid (J ² /m ⁴ /s ¹ /K ²)	κ_D Liquid (m ² /s)	$\lambda_{th} \cdot \rho \cdot c_p$ Liquid (J ² /m ⁴ /s ¹ /K ²)	c_s Liquid (m/s)
Al	9.7×10^{-5}	5.8×10^8	3.6×10^{-5}	2.8×10^8	4561
Au	1.3×10^{-4}	7.9×10^8	4.2×10^{-4}	2.9×10^8	2567
Cu	1.2×10^{-4}	1.4×10^9	4.2×10^{-5}	6.5×10^8	3440
Fe	2.3×10^{-5}	2.8×10^8	5.7×10^{-6}	1.8×10^8	4200
Ti	9.3×10^{-6}	5.2×10^7	8.6×10^{-6}	9.1×10^7	4407
W	6.8×10^{-5}	4.4×10^8	3.7×10^{-5}	3.3×10^8	3000
Zn	4.2×10^{-5}	3.2×10^8	2.4×10^{-5}	1.5×10^8	2850

References

- Hügel, H.; Graf, T. *Materials Processing with Lasers, Fundamentals and Procedures*, 1st ed.; Springer: Wiesbaden, Germany, 2026.
- Kawahito, Y.; Wang, H.; Katayama, S.; Sumimori, D. Ultra high power (100 kW) fiber laser welding of steel. *Opt. Lett.* **2017**, *43*, 4667–4670. [\[CrossRef\]](#)
- Speker, N.; Haug, P.; Feuchtenbeiner, S.; Hesse, T.; Havrilla, D. BrightLine weld-spatter reduced high speed welding with disk lasers. In *Proceedings Volume 10525, High-Power Laser Materials Processing: Applications, Diagnostics, and Systems VII*; SPIE: Bellingham, WA, USA, 2018; p. 105250C. [\[CrossRef\]](#)
- Papastathopoulos, E.; Bocksrocker, O.; Fiechtner, K.; Pricking, S.; Flaig, R.; Effinger, O.; Ryba, T. Advances in beam shaping of high-power CW lasers with BrightLine weld technology. In *Proceedings Volume 11994, High-Power Laser Materials Processing: Applications, Diagnostics, and Systems XI*; SPIE: Bellingham, WA, USA, 2022; p. 1199402. [\[CrossRef\]](#)
- Punzel, E.; Hugger, F.; Dörringer, R.; Dinkelbach, T.L.; Bürger, A. Comparison of different system technologies for continuous-wave laser beam welding of copper. *Procedia CIRP* **2020**, *94*, 587. [\[CrossRef\]](#)
- Rinne, J.; Nothdurft, S.; Hermsdorf, J.; Kaierle, S.; Overmeyer, L. Multivariate parametric study on laser beam welding of copper lap joints using adjustable intensity profiles. *Procedia CIRP* **2022**, *111*, 415. [\[CrossRef\]](#)
- Kaufmann, F.; Maier, A.; Schrauder, J.; Roth, S.; Schmidt, M. Influence of superimposed intensity distributions on weld seam quality and spatter behavior during laser beam welding of copper with green laser radiation. *J. Laser Appl.* **2022**, *34*, 042008. [\[CrossRef\]](#)
- Fabbro, R.; Chouf, K. Keyhole modeling during laser welding. *J. Appl. Phys.* **2000**, *87*, 4075–4083. [\[CrossRef\]](#)
- Fabbro, R.; Slimani, S.; Coste, F.; Briand, F. Study of keyhole behaviour for full penetration Nd-Yag CW laser welding. *J. Phys. D Appl. Phys.* **2005**, *38*, 1881–1887. [\[CrossRef\]](#)
- Hansen, K.S.; Kristiansen, M.; Olsen, F.O. Beam Shaping to Control of Weldpool Size in Width and Depth. *Phys. Procedia* **2014**, *56*, 467–476. [\[CrossRef\]](#)
- Masanori, M.; Zhang, X.; Kawahito, Y.; Katayama, S. Development of spatter suppression technology for copper by high speed laser scanner welding. In *International Congress on Applications of Lasers & Electro-Optics*; Laser Institute of America: Orlando, FL, USA, 2015; pp. 544–548. [\[CrossRef\]](#)
- Hansen, K.S.; Olsen, F.O.; Kristiansen, M.; Madsen, O. Inline Repair of Blowouts During Laser Welding. *Phys. Procedia* **2017**, *89*, 58–69. [\[CrossRef\]](#)
- Falk, N.; Lucas, B.; Pierre, B.J. Description of the influence of two laser intensities on the spatter formation on laser welding of steel. *Procedia CIRP* **2018**, *74*, 475–480. [\[CrossRef\]](#)
- Florian, F.; Sommer, M.; Weber, R.; Weberpals, J.-P.; Graf, T. Reduction of pores by means of laser beam oscillation during remote welding of AlMgSi. *Opt. Lasers Eng.* **2018**, *108*, 68–77. [\[CrossRef\]](#)
- Zenz, C.; Buttazzoni, M.; Cenicerros, M.M.; Vázquez, R.G.; Puchades, J.R.B.; Griñán, L.P.; Otto, A. Simulation-based process optimization of laser-based powder bed fusion by means of beam shaping. *Addit. Manuf.* **2023**, *77*, 103793. [\[CrossRef\]](#)

16. Levichev, N.; Herwig, P.; Wetzig, A.; Duflou, J.R. Towards robust dynamic beam shaping for laser cutting applications. *Procedia CIRP* **2022**, *111*, 746. [[CrossRef](#)]
17. Kumar, A.; Duran, C.; Couso, E.V.; Orioux, A.; Pallier, G.; Lemaitre, D.; Otto, A.; Labroille, G.; Nuzhdin, D. Advanced beam shaping strategies studied via simulation and testing to enhance laser welding processes in the e-mobility sector. In *Proceedings Volume 13886, High-Power Laser Materials Processing: Applications, Diagnostics, and Systems XV*; SPIE: Bellingham, WA, USA, 2026; p. 138860F. [[CrossRef](#)]
18. Bayat, M.; Rothfelder, R.; Schwarzkopf, K.; Zinoviev, A.; Zinovieva, O.; Spurk, C.; Hummel, M.; Olowinsky, A.; Beckmann, F.; Schmidt, J.M.M. Exploring spatial beam shaping in laser powder bed fusion: High-fidelity simulation and in-situ monitoring. *Addit. Manuf.* **2024**, *93*, 104420. [[CrossRef](#)]
19. Bakhtari, A.R.; Sezer, H.K.; Canyurt, O.E.; Eren, O.; Shah, M.; Marimuthu, S.A. Review on Laser Beam Shaping Application in Laser-Powder Bed Fusion. *Adv. Eng. Mater.* **2024**, *26*, 2302013. [[CrossRef](#)]
20. Schmidt, M.; Cvecek, K.; Duflou, J.; Vollertsen, F.; Arnold, C.B.; Matthews, M.J. Dynamic beam shaping—Improving laser materials processing via feature synchronous energy coupling. *CIRP Ann.* **2024**, *73*, 533–559. [[CrossRef](#)]
21. Jabar, S.; Pamarthi, V.V.; Hayat, Q.; Khan, M.H.; Kotadia, H.R.; Franciosa, P. A review of beam shaping approaches for near-infrared continuous-wave laser welding in e-mobility applications. *Opt. Laser Technol.* **2025**, *192*, 114000. [[CrossRef](#)]
22. Eyal, S.; Yaniv, V.; Benayahu, U. 16kW Single Mode CW Laser with Dynamic Beam for Material Processing. In *Proceedings Volume 11260, Fiber Lasers XVII: Technology and Systems*; SPIE: Bellingham, WA, USA, 2020; p. 1126021. [[CrossRef](#)]
23. Wagner, J.; Heider, A.; Ramsayer, R.; Weber, R.; Faure, F.; Leis, A.; Armon, N.; Susi, R.; Tsiony, O.; Shekel, E.; et al. Influence of dynamic beam shaping on the geometry of the keyhole during. In *Proceedings of the 12th CIRP Conference on Photonic Technologies [LANE 2022]*, Fürth, Germany, 4–8 September 2022. [[CrossRef](#)]
24. Heider, A.; Weber, R.; Graf, T.; Herrmann, D.; Herzog, P. Power Modulation to Stabilize Laser Welding of Copper. *J. Laser Appl.* **2015**, *27*, 022003. [[CrossRef](#)]
25. Maiwald, D.; Nothdurft, S.; Hermsdorf, J.; Kaierle, S. Deep penetration welding of brass with subsequent wire filling process by laser beam with combined core and ring beam. *Procedia CIRP* **2024**, *124*, 399–402. [[CrossRef](#)]
26. Kumar, A.; Meunier, M.; Gaillard, N.; Lemaitre, D.; Pallier, G.; Labroille, G. An optimal tailored beam-shape to improve copper welding with a 1µm 8kW laser. In *Proceedings Volume PC12414, High-Power Laser Materials Processing: Applications, Diagnostics, and Systems XII*; SPIE: Bellingham, WA, USA, 2023; p. PC1241409. [[CrossRef](#)]
27. Rumble, J.R. (Ed.) *CRC Handbook of Chemistry and Physics*, 106th ed.; CRC Press: Boca Raton, FL, USA, 2025.
28. Leitner, M.; Leitner, T.; Schmon, A.; Aziz, K.; Pottlacher, G. Thermophysical Properties of Liquid Aluminum. *Metall. Mater. Trans. A* **2017**, *48*, 3036–3045. [[CrossRef](#)]
29. Blairs, S.; Joasoo, U. Sound velocity and compressibility in liquid metals. *J. Inorg. Nucl. Chem.* **1980**, *42*, 1555–1558. [[CrossRef](#)]
30. Casas, J.; Kéita, N.M.; Steinemann, S.G. Sound Velocity in Liquid Titanium, Vanadium and Chromium. *Phys. Chem. Liq.* **1984**, *14*, 155. [[CrossRef](#)]
31. Hixson, R.S.; Winkler, M.A. Thermophysical Properties of Solid and Liquid Tungsten. *Int. J. Thermophys.* **1990**, *11*, 709. [[CrossRef](#)]
32. Zhao, C.; Parab, N.D.; Li, X.; Fezza, K.; Tan, W.; Rollett, A.D.; Sun, T. Critical instability at moving keyhole tip generates porosity in laser melting. *Science* **2020**, *370*, 1080. [[CrossRef](#)] [[PubMed](#)]
33. Weber, R.; Wagner, J.; Peter, A.; Hagenlocher, C.; Spira, A.; Urbach, B.; Shekel, E.; Vidne, Y. Basic properties of high-dynamic beam shaping with coherent combining of high-power laser beams for materials processing. *J. Manuf. Mater. Process.* **2025**, *9*, 85. [[CrossRef](#)]
34. Armon, N.; Tsiony, O.; Cohen, R.; Greenberg, E.; Assa, R.; Shekel, E. Controlling weld quality in thick steel sections: A combined experimental and simulation study using dynamic beam lasers. *Weld. World* **2025**, preprint. [[CrossRef](#)]

Disclaimer/Publisher's Note: The statements, opinions and data contained in all publications are solely those of the individual author(s) and contributor(s) and not of MDPI and/or the editor(s). MDPI and/or the editor(s) disclaim responsibility for any injury to people or property resulting from any ideas, methods, instructions or products referred to in the content.